THREE-DIMENSIONAL NUMERICAL GAS FLOW MODELLING OF BOILER FURNACES

R.K. BOYD   AND   J.H. KENT

THE ELECTRICITY COMMISSION OF N.S.W.

SYDNEY 2000 AUSTRALIA

DEPARTMENT OF MECHANICAL ENGINEERING

UNIVERSITY OF SYDNEY

N.S.W. 2006 AUSTRALIA

SUMMARY This paper describes preliminary results of a project whose aim is to model a pulverised fuel fired boiler furnace. A three-dimensional finite difference code developed at Imperial College is being applied to the Liddell Power Station boiler furnace. When complete the model will predict furnace gas flow, combustion and heat transfer and should give an insight into the effects of parametric influences upon flow patterns and flame stability and provide a powerful tool for furnace design. The present paper outlines the approach and describes the work carried out so far. Isothermal flow predictions have been made for the Liddell furnace and flow patterns are presented for various burner inlet conditions, some of which are compared with full scale boiler experimental data.

1.   INTRODUCTION

A majority of the pulverised coal fired boilers currently being operated by the Electricity Commission of NSW are "tangentially" corner fired designs with consequent turbulent, highly recirculating and non-symmetrical flows in the burner regions. The capital cost and operation of these boilers is high and the expenditure required for experimenting with design modifications to existing plant is prohibitive. In the past furnace designers have been forced to be satisfied with cold airflow scale models which neglect the complex combustion processes and unique NSW coal properties. Hence an analytical model able to predict furnace flow, combustion and heat transfer would be invaluable from design and operational viewpoints.

Combustion, flow and heat transfer modelling has been carried out previously, although most researchers have concentrated upon test and industrial furnaces with relatively simple geometries. An excellent review of existing models has been made by McDonald (1979).

The present paper describes a project currently being conducted to develop a finite difference flow combustion and heat transfer model of one of ECNSW's Liddell Power Station 500 MW (electrical) boilers. The numerical code used is based upon a version of the TEACH code developed at Imperial College for the solution of three-dimensional recirculating and turbulent flows. The solution procedure and application are described and initial results of isothermal flow conditions presented and compared with experimental data. Results of a sensitivity analysis performed to determine the relationship between the inlet conditions and the solution flow field are also given.

2.   THE MODELLED BOILER

The boiler considered for this study is one of the four identical 500 MW (electrical) pulverised coal fired units being operated by ECNSW at the Liddell Power Station. Each tower boiler comprises two rectangular vertical furnaces having a common central water wall.

Each furnace is fired from four sets of burners in a tangential arrangement as shown in Figures 1 and 2. Each burner set consists of eight pulverised coal and primary air entry ports which are surrounded above and below by secondary air ports which supply approximately 80% of the combustion air (see Figure 3). To achieve a swirling flow pattern the burner ports are directed toward the central region of the furnace. A vertical section through the furnace (Figure 2) extending from the bottom of the boiler to the start of the super-heater stages shows the locations of the pulverised coal burners.

3.   THE NUMERICAL CODE

The TEACH code which provides the basis of the model used here, has been used for many models of both two- and three-dimensional flows in gas, oil and coal fired furnaces. Exponents of TEACH include Khalil et al. (1975), Abbas et al. (1981) and Carvalho and Lockwood (1981). The derivation of the finite difference equations and the solution procedure have been explained in detail by Gosman and Ideriah (1976) and thus only a brief description of TEACH appears below.

Since knowledge of the fine scale fluctuations of the variables is not required and would be prohibitive to compute due to the number of equations involved, the 2-equation k-ε turbulence model is used. This model has been well tested and has proved to be a good compromise between computational economy and accuracy. A detailed description of the k-ε turbulence model is presented by Launder and Spalding (1972).

The differential equations governing the transport of flow properties are presented below for cartesian coordinates. The momentum equation in the x-direction for the u-velocity component is:

$$\frac{\partial}{\partial x}\left(\rho u^2 - \mu_{eff}\frac{\partial u}{\partial x}\right) + S_u = 0$$

where μ_{eff}, the effective viscosity is a combination of the laminar and turbulent viscosities. The source term S_u is given by:

$$S_u = -\frac{\partial p}{\partial x} + \frac{\partial}{\partial x}\left(\mu_{eff}\frac{\partial u}{\partial x}\right) + \frac{\partial}{\partial y}\left(\mu_{eff}\frac{\partial v}{\partial x}\right) + \frac{\partial}{\partial z}\left(\mu_{eff}\frac{\partial w}{\partial x}\right) .$$

where v and w are the velocity components in the y and z directions respectively.

The turbulence energy k is governed by:

$$\frac{\partial}{\partial x}(\rho uk) + \frac{\partial}{\partial y}(\rho vk) + \frac{\partial}{\partial z}(\rho wk) =$$

$$\frac{\partial}{\partial x}\left(\mu_{eff}\frac{\partial k}{\partial x}\right) + \frac{\partial}{\partial y}\left(\mu_{eff}\frac{\partial k}{\partial y}\right) + \frac{\partial}{\partial z}\left(\mu_{eff}\frac{\partial k}{\partial z}\right) + S_k = 0$$

where the source term S_k is given by $S_k = G - \rho\varepsilon$ and

G the turbulence generation term:

$$G = \mu_{eff}\left\{2\left[\left(\frac{\partial u}{\partial x}\right)^2 + \left(\frac{\partial v}{\partial y}\right)^2 + \left(\frac{\partial w}{\partial z}\right)^2\right] + \left(\frac{\partial u}{\partial y} + \frac{\partial v}{\partial x}\right)^2 \right.$$

$$\left. + \left(\frac{\partial v}{\partial x} + \frac{\partial w}{\partial y}\right)^2 + \left(\frac{\partial u}{\partial z} + \frac{\partial w}{\partial x}\right)^2\right\}$$

The energy dissipation ε is governed by:

$$\frac{\partial}{\partial x}(\rho u \varepsilon) + \frac{\partial}{\partial y}(\rho v \varepsilon) + \frac{\partial}{\partial z}(\rho w \varepsilon) =$$

$$\frac{\partial}{\partial x}\left(\frac{\mu_{eff}}{1.22}\frac{\partial}{\partial x}\right) + \frac{\partial}{\partial y}\left(\frac{\mu_{eff}}{1.22}\frac{\partial \varepsilon}{\partial y}\right) + \frac{\partial}{\partial x}\left(\frac{\mu_{eff}}{1.22}\frac{\partial \varepsilon}{\partial z}\right) + S_\varepsilon = 0$$

and the source term $S_\varepsilon = \frac{\varepsilon}{k}\left(1.44\ G - 1.92\ \rho\varepsilon\right)$.

The furnace is subdivided into a number of control volumes or cells, each of which encloses an imaginary grid node where all of the scalar dependent variables are calculated. At the scalar cell boundaries, the 3 velocity components are calculated according to the 'staggered grid' arrangement (see Gosman and Ideriah, 1976).

A finite difference technique is employed to solve the conservation equations for momentum and scalar transport at each cell. Since no pressure transport equation exists, the SIMPLE algorithm is used to close the system of equations. A pressure field is presumed and a first approximation of the velocity field is obtained. Subsequent corrections are applied to the pressure field so as to bring the velocity field into conformity with the continuity equation. This procedure is repeated until the error or residual mass in each cell falls below a specified value.

The finite difference equations are solved by the Tri-Diagonal Matrix Algorithm (TDMA). This procedure is applied successively to the x lines and then the y lines in each x-y plane in turn. Thus the calculation domain is repeatedly swept plane by plane from the base of the furnace to the exit until a solution is reached.

4.   THE APPLICATION OF TEACH

For the initial isothermal model developed for this study, only the main furnace region was modelled. This region extended from the bottom of the boiler to a plane immediately upstream of the superheater tube banks. Approximations were made to minimise the number of nodes whilst simulating the main aerodynamic features as accurately as possible.

4.1   Convergence Criteria

The iterative solution procedure of the finite difference equations is terminated when the solution has reached 'convergence'. To test for convergence the absolute values of the residual sources of each transport equation were summed after first being normalised by the respective inlet variable values. This was performed at each iteration, the solution being considered converged when this summation fell below 0.001.

4.2   The Computational Mesh

The grid which was found to provide sufficient flow information was a 12×10×11 node mesh as shown in Figure 4. In the x-y planes a relatively fine mesh was used in the burner regions since high velocity gradients are present near the issuing jets. Convergence proved to be very slow with a coarse mesh. In the x-direction the fineness proved to be much more critical for convergence than in the y-direction since the burner jet v-momentum predominates and higher velocity gradients are present in regions on each side of the entry ports.

In the vertical (z) direction a relatively fine mesh was again needed in the burner region to improve the rate of convergence. With the decreasing velocity gradients downstream of the burners the z spacings could be increased.

4.3   Boundary Conditions

Since the furnace walls are steel tubed water walls no special boundary conditions were required for the isothermal flow study - the standard TEACH methods were used (see Gosman and Ideriah, 1976). For the solution field of each variable, depending upon the distance of the node from the wall, either a one-dimensional laminar flow or turbulent flow is assumed.

4.4   Burner Treatment

Each vertical burner group (as shown in Figure 3) is segmented into small ports for the entry of secondary air, pulverised fuel and ignition oil. To avoid grid intricacies, the burners and air ports were approximated as one vertical slit-shaped inlet region. To enable a cartesian mesh to be retained, these inlet slits were located flush with the front or rear walls and not in wall indentations aimed towards the centre of the furnace. These indentations were assumed to have little effect on the large scale furnace flow pattern. Care was taken to ensure that the burner centrelines were located as accurately as possible. Since the burner pairs 1,4 and 2,3 do not lie precisely opposite each other and to avoid an extremely fine mesh this could only be achieved to within 50 mm. After altering the burner locations slightly it was found that the solution field was quite insensitive to small perturbations to the inlet port locations.

Each inlet port comprised one scalar cell in width and six in height; thus each burner group was simulated by a planar jet having a perfectly flat velocity profile. The burner port was not discretised more than this since the flow pattern was assumed to be dependent upon the combined effect of the four inlet streams rather than fine scale flows occurring within the inlet jets.

To represent the mass flow from the angled inlet ports, the inlet cell boundary conditions were modified via the source terms of the transport equations for each variable. If $\dot{M}_{ic}$ is the mass flowrate per unit height of a typical inlet port, then Δx, Δy, u_{ic} and v_{ic}, as defined in Figure 5, must be selected to ensure that the correct mass flowrate is obtained:

$$\rho v_{ic}\ \Delta x + u_{ic}\ \Delta y = \dot{M}_{ic}$$

The angular relationship of the momentum components must satisfy:

$$\frac{\rho u_{ic}^2\ \Delta y}{\rho v_{ic}^2\ \Delta x} = \tan\theta$$

so that the actual angle θ of the burner to the centreline is achieved.

For the isothermal Liddell model described here, Δx was chosen to be 0.55 m, which is approximately equal to the projected port width onto the boiler wall; thus the dimensions of the issuing jet, the velocities and the gradients were all approximately conserved.

To impose the inlet port boundary conditions upon the calculation procedure the momentum equations and continuity equations had extra source terms added. Momentum fluxes of $\rho u_{ic}^2\ \Delta y$ and $\rho v_{ic}^2\ \Delta x$ were added to the v-momentum and u-momentum source terms respectively. For each variable calculation a mass source of $\dot{M}_{ic}\ \Delta z$ was included in the continuity equation.

4.5 Liddell Tests

For comparison with the isothermal model results, data was obtained during cold airflow testing of the Liddell boiler. A three-dimensional hotwire anemometer with 25.0μm platinum wires was used to measure air velocities along with a cotton tuft to aid in the direction determination. Two planes in the burner region and one at the furnace outlet were traversed, with approximately 45 locations being monitored at each plane. The boiler forced draught and induced draught fans were operated, resulting in secondary air only being supplied to the boiler at the boiler 'constant maximum rating' mass flow.

5. RESULTS

The code was run on a VAX-11 computer for the grid and boundary conditions described earlier, with numerical solutions being obtained for u, v, w, k and ε. The inlet conditions were chosen to simulate the testing described in §4.5. This corresponded to a furnace gas mass flowrate of 210 kgs^{-1} and a consequent burner jet velocity of 10.5 ms^{-1} for air at ambient temperature.

After experimenting with various mesh spacings a 12×10×11 node grid was found to give grid independent solutions. With this grid each iteration of the solution took 17 s with between 100 and 140 iterations being required for convergence depending upon the inlet conditions.

5.1 Comparison with Measured Results

Results obtained from the model for inlet conditions equivalent to secondary airflow only and equal mass flows from all four burners are presented graphically in Figure 6a. The vector diagram presented is for the top burner level and is indicative of the flow pattern present at any of the burner levels. Due to the higher tangential momentum component of the 40° burners the flow direction is clockwise (when viewed from above) forming a large swirl pattern. The individual burner jets only extend 1 to 2 metres into the furnace before joining the main flow streams.

The measured flow pattern obtained with the hotwire anemometer at the top burner level are presented in Figure 6b. These values are not of high accuracy due to the high turbulence levels and the subsequent problems in observing the tuft; nevertheless the measured flow field is in good agreement with the predicted results.

At the furnace outlet the flow field is an important consideration since gas velocities here will influence the superheater tube metal temperatures (a limiting factor in boiler operation) and regions where tube erosion is likely to occur. The predicted furnace outlet velocity profile for equal flow from all four inlet ports is presented in Figure 7b. At the centre of the swirl the w (vertical) velocity component is relatively low as can be seen by the depression in the velocity profile. Surrounding this low velocity region is an elliptical shaped ridge oriented towards corners 1 and 3. Corners 2 and 4 have peaks in w-velocity, since the streams from the 28° burners (1 and 3) are directed into these corners (see Figure 6a). The high velocities in these corners are supported by high temperature and heat flux measurements during actual boiler operation. The velocity profile obtained with the hotwire anemometer (Figure 8) shows a similar central depression to the predicted results, but peaks occur in all four corners rather than in corners 2 and 4 only. In an effort to explain this anomaly the sensitivity of the model to various furnace inlet conditions was examined.

5.2 Sensitivity to Furnace Inlet Conditions

Due to the geometry of the secondary air ducting to the four burner sets, the mass flowrates to each of the burners is unlikely to be perfectly equal. Thus the model was used to investigate the effects of varying the mass flow balance between the four inlet ports. The modelled conditions included higher mass flows from one, two and three of the burners whilst maintaining the total mass flow at a constant rate.

The results of this analysis showed that altering the inlet conditions has a noticeable effect on the flow in the burner region and a significant effect on the furnace outlet velocity profile. The greatest change in the flow pattern occurred when the mass flow from the 28° burners (1 and 3) was increased by 15% and the flow from the 40° burners dropped by 15% (Figure 9a). In the burner planes only a small swirling zone was present in the centre of the furnace with recirculation zones occurring between the burners and the side walls. This change in the flow pattern near the burners resulted in an outlet velocity profile with a large central peak and low regions near the side walls (Figure 9b).

The results obtained by increasing the mass flow from the 40° ports by 15% are presented in Figure 10. The elliptical flow pattern in the outlet plane has its long axis parallel to the furnace front and rear walls rather than extending from corner 1 to corner 3 as in the equal mass flow case. Thus the outlet velocity profile proved to have 10% lower peaks in corners 2 and 4 and 20% higher w-velocities in corners 1 and 3 (Figure 10c).

With higher mass flows from burners 1 and 2 (Figure 11a) a 20% lower velocity peak resulted in corner 2 along with a broader peak in corner 4 extending along the side wall. Little change over the equal mass flow case was evident (Figure 11b) with 15% higher mass flows from burners 2 and 3, apart from a more uniform velocity distribution along the right side wall. Both of these conditions presented in Figure 11 show marked asymmetry in the outlet velocity profile.

6. CONCLUSIONS

The isothermal furnace simulation and the results obtained with the hotwire anemometer show good agreement which is encouraging considering the complexity of three-dimensional recirculating flows. The sensitivity analysis of the inlet mass flow balance from the four burners provides an insight into how specific operating problems such as high metal temperatures and tube erosion may arise.

In particular, from this preliminary study it appears that the maintenance of equal burner mass flows is more important than previously believed and specific attention should be made to ensure that the 28° burners do not have excessive mass flows. This will be confirmed by further cold airflow testing in due course.

7. ACKNOWLEDGEMENTS

8. REFERENCES

CARVALHO, M. and LOCKWOOD, F.C. (1981) Prediction of Combustion of an End Wall Fired Glass Furnace. Internal Report, Mech. Eng. Dept., Imperial College.

GOSMAN, A.D. and IDERIAH, F.J.K. (1976) TEACH-T: A General Computer Program for Two-Dimensional, Turbulent Recirculating Flows. Fluids Section Report, Mech. Eng. Dept., Imperial College.

KHALIL, E.E., SPALDING, D.B. and WHITELAW, J.H. (1975) The Calculation of Local Flow properties in a Two-Dimensional Furnace. Int. J. Heat Mass Transfer, 18, pp. 775-791, Pergamon Press.

LAUNDER, B.E. and SPALDING, D.B. (1972) Mathematical Models of Turbulence. Academic Press, London and New York.

McDONALD, H. (1972) Combustion Modelling in 2 and 3 Dimensions - Some Numerical Considerations. Prog. Energy Combustion Sci., pp. 97-122.

9. FIGURES

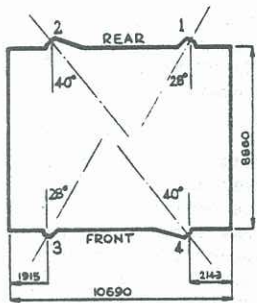$\downarrow \equiv \uparrow \_10 \text{ms}^{-1}$ In all vector diagrams.

FIGURE 1. Plan view of tangential firing arrangement
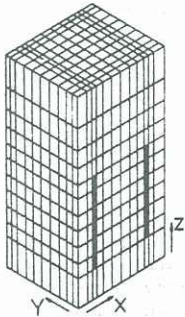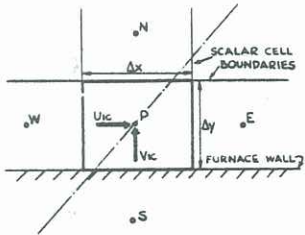

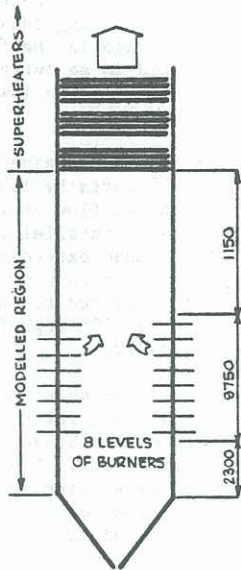FIGURE 4. The Computational Mesh

FIGURE 5. Inlet cell details

FIGURE 2. Vertical elevation of furnace
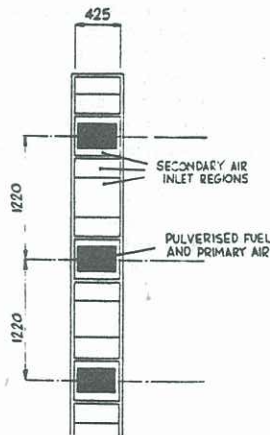
FIGURE 3. Burner details. Only top 3 levels are shown.
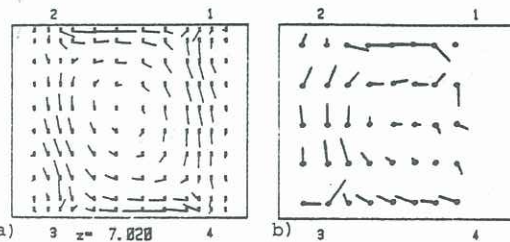
FIGURE 6. Burner plane velocity vectors for equal mass flows. a) model predictions b) anemometer measurements
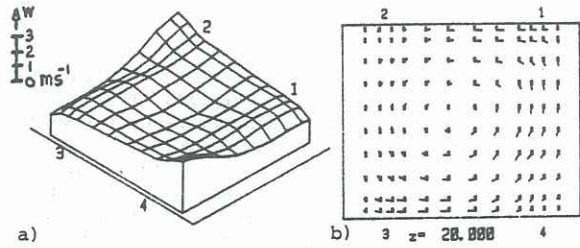
FIGURE 7. Equal burner mass flows. a) outlet velocity profile; b) outlet plane velocity vectors
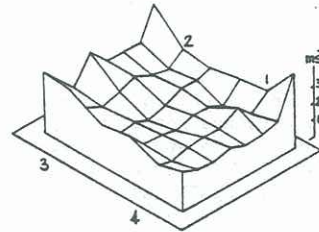

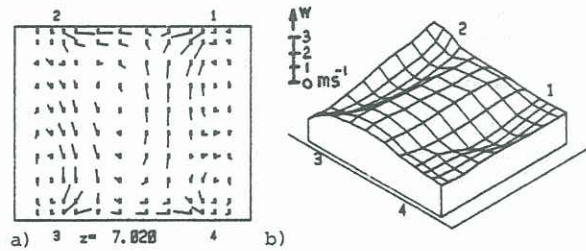FIGURE 8. Furnace outlet velocity profile obtained with hotwire anemometer

FIGURE 9. 15% higher mass flows from ports 1 & 3 a) burner plane vectors; b) outlet velocity profile.
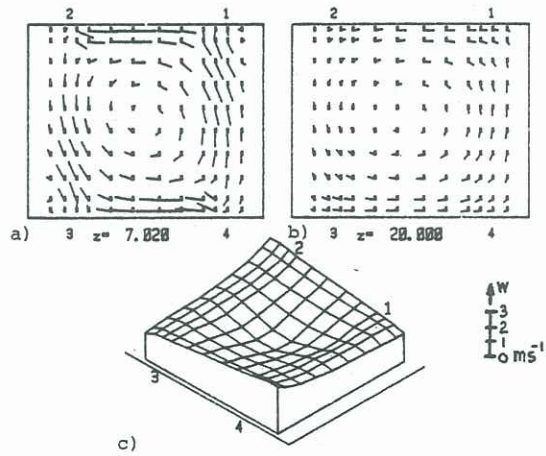

FIGURE 10. 15% Higher mass flows from ports 2 & 3 a) burner plane vectors; b) outlet plane vectors c) outlet profile.
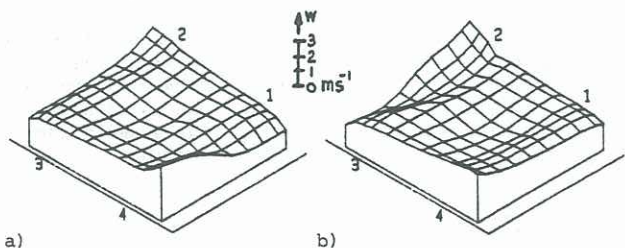

FIGURE 11. Outlet velocity profiles for a) 15% higher flows from ports 1&2; b) 15% higher flows from ports 2&3